HAL open science

Approximate observability and back and forth observer of a PDE model of crystallisation process

Lucas Brivadis, Ludovic Sacchelli

To cite this version:

Lucas Brivadis, Ludovic Sacchelli. Approximate observability and back and forth observer of a PDE model of crystallisation process. CDC 2021 - 60th IEEE Conference on Decision and Control, Dec 2021, Austin, Texas, United States. pp.4436-4441, 10.1109/CDC45484.2021.9683245 . hal-03175017

HAL Id: hal-03175017

https://hal.science/hal-03175017v1

Submitted on 19 Mar 2021

HAL is a multi-disciplinary open access archive for the deposit and dissemination of scientific research documents, whether they are published or not. The documents may come from teaching and research institutions in France or abroad, or from public or private research centers.

L'archive ouverte pluridisciplinaire **HAL**, est destinée au dépôt et à la diffusion de documents scientifiques de niveau recherche, publiés ou non, émanant des établissements d'enseignement et de recherche français ou étrangers, des laboratoires publics ou privés.

Approximate observability and back and forth observer of a PDE model of crystallisation process

Lucas Brivadis and Ludovic Sacchelli

***Abstract*— In this paper, we are interested in the estimation of Particle Size Distributions (PSDs) during a batch crystallization process in which particles of two different shapes coexist and evolve simultaneously. The PSDs are estimated thanks to a measurement of an apparent Chord Length Distribution (CLD), a measure that we model for crystals of spheroidal shape. Our main result is to prove the approximate observability of the infinite-dimensional system in any positive time. Under this observability condition, we are able to apply a Back and Forth Nudging (BFN) algorithm to reconstruct the PSD.**

I. Introduction

During a batch crystallization process, a critical issue is to monitor the Particle Size Distribution (PSD), which may affect the chemical-physical properties of the product. In particular, multiple types of crystals may be evolving simultaneously in the reactor, with stable and meta-stable crystal formations. In that case, estimating the PSD associated to each shape is an important task, but difficult to realize in practice. Modern Process Analytical Technologies (PATs) offer a wide variety of approaches to extract PSD information from measurements, such as image processing based methods [11], [22] for instance. The use dynamical observers is a popular approach to the issue [7], [12], [15], [18], [21], [25], [26]. A particular technique, on which we focus in this article, is to use PATs giving access to the Chord Length Distribution (CLD) (such as the Focused Beam Reflectance Measurement or the BlazeMetrics® technologies), and to reconstruct the PSD from the knowledge of the CLD [1], [16], [20], [27]. When scanning across crystals, these sensors actually measure chords on the projection of the crystal on the plane that is orthogonal to the probe. Hence, the measured CLD highly depends on the shapes that the crystals in the reactor may take. And in many crystallization processes, several shapes can coexist due to polymorphism. Since the CLD sums up the contribution of each shape in one measurement, recovering the PSD associated to each shape only from the common CLD is a major challenge not yet tackled by the existing literature.

In the previous work [8], we proposed: *(i)* a model of the PSD-to-CLD relation for spheroid particles; *(ii)* a direct inversion method to instantly recover the PSD from the CLD when all particles have the same shape; *(iii)* a back and forth observer to reconstruct the PSD of several shapes from the knowledge of their common CLD on a finite time interval and an evolution model of the process. We were able to prove the convergence of the algorithm only in one case: when crystals have only two possible shapes (spheres and elongated spheroids of fixed eccentricity), each having a positive growth rate independent of the size (McCabe hypothesis). Among the differences with the previous result, let us highlight the two main improvements of this paper: *(a)* we consider size-dependent growth rates; *(b)* we consider almost all possible combinations of two spheroid shapes with different eccentricities. Then, we perform an observability analysis of the infinite-dimensional system, which is the main result of the paper.

This research was partially funded by the French Grant ANR ODISSE (ANR-19-CE48-0004-01)

L. Brivadis and L. Sacchelli are with Univ. Lyon, Université Claude Bernard Lyon 1, CNRS, LAGEPP UMR 5007, 43 bd du 11 novembre 1918, F-69100 Villeurbanne, France lucas.brivadis@univ-lyon1.fr, ludovic.sacchelli@univ-lyon1.fr

II. Evolution model and CLD

A spheroid is a surface of revolution, obtained by rotating an ellipse along one of its axes of symmetry. In particular, spheres are spheroids. A spheroid is fully described by two scalar parameters: a radius r, characterizing its size and being the radius that is orthogonal to its rotation's axis, and an eccentricity η, characterizing its shape and being the ratio between the radius along its rotation's axis and r.

Consider a batch crystallisation process during which crystals of only two shapes appear: spheroids of eccentricities η_1 and η_2. Let ψ_1 and ψ_2 be their corresponding PSDs. At any time $t \in [0, T]$ during the process, $\int_{r_1}^{r_2} \psi_i(t, r)\mathrm{d}r$ is the number of crystals per unit of volume at time t having the shape η_i and a radius r between r_1 and r_2.

Let $r_i^{\min}$ be the minimal size at which crystals of shape η_i appear and $r_i^{\max}$ be a maximal radius that no crystals can reach during the process. At time $t = 0$, assume that seed particles with PSD $\psi_{i,0}$ for each shape η_i lie in the reactor. Denote by $G_i(t, r)$ the grow rate of crystals of shape η_i and size r at time t. The usual (see, *e.g.*, [17], [19]) population balance equation leads to

$$\frac{\partial \psi_i}{\partial t}(t, r) + G_i(t, r)\frac{\partial \psi_i}{\partial r}(t, r) = 0 \tag{1}$$

Assume that G_i is C^1. Note that the growth rate may be positive or negative. The boundary conditions are given by

$$\psi_i(t, r_i^{\min}) = u_i(t) \tag{2}$$

$$\psi_i(t, r_i^{\max}) = 0 \tag{3}$$

where $u_i(t)$ denotes the appearance of particles of size $r_i^{\inf}$ and shape η_i at time t. Since u_i is supposed to be unknown, it is part of the data to be estimated, with $\psi_{i,0}$. Note that the

boundary conditions impose a relation between u_i and $\psi_{i,0}$ when $G_i(t, r_i^{\min}) < 0$. Set

$$r_i^{\inf} = \min\left\{r_i^{\min}, r_i^{\min} - \max_{\tau\in[0,T]} \int_0^\tau G_i(t, r_i^{\min})\mathrm{d}t\right\} \quad (4)$$

$$r_i^{\sup} = \max\left\{r_i^{\max}, r_i^{\max} - \min_{\tau\in[0,T]} \int_0^\tau G_i(t, r_i^{\max})\mathrm{d}t\right\} \quad (5)$$

In order to ensure the well-posedness of the evolution equation, let us define $\psi_i(t, r)$ and $G_i(t, r)$ for $t \in [0, T]$ and $r \in [r_i^{\inf}, r_i^{\sup}] \setminus [r_i^{\min}, r_i^{\max}]$ by

$$\begin{cases} \psi_i(t, r) = u_i(t + \tau), \\ G_i(t, r) = G_i(t, r_i^{\min}), \end{cases} \quad \forall r \in [r_i^{\inf}, r_i^{\min}] \quad (6)$$

$$\begin{cases} \psi_i(t, r) = 0, \\ G_i(t, r) = G_i(t, r_i^{\max}), \end{cases} \quad \forall r \in [r_i^{\max}, r_i^{\sup}] \quad (7)$$

where τ in (6) is such that

$$r_i^{\min} = r + \int_t^{t+\tau} G_i(s, r_i^{\min})\mathrm{d}s \quad (8)$$

Roughly speaking, $\psi_i(t, r)$ for $r < r_i^{\min}$ represents crystals that did not yet appear at time t, but will appear later at some time $t + \tau$.

Then the evolution of the crystallization process can be modeled as

$$\begin{cases} \dfrac{\partial \psi_i}{\partial t}(t, r) + G_i(t, r)\dfrac{\partial \psi_i}{\partial r}(t, r) = 0 \\ \psi_i(0, r) = \psi_{i,0}(r) \end{cases} \quad (9)$$

where $i \in \{1, 2\}$, $t \in [0, T]$, $r \in [r_i^{\inf}, r_i^{\sup}]$ and with the periodic boundary condition $\psi_i(t, r_i^{\inf}) = \psi_i(t, r_i^{\sup})$ since the boundary terms does not influence $\psi_i(t, r)$ for $r \in [r_i^{\min}, r_i^{\max}]$ and $t \leq T$. The new initial condition $\psi_{i,0}(r)$ contains both the information on the seed particles (for $r \in [r_i^{\min}, r_i^{\max}]$ and on all the crystals that will appear during the process (for $r \in [r_i^{\inf}, r_i^{\min}]$).

Note that, contrary to [8], we do not assume that $r_1^{\min} = r_2^{\min}$, nor that $G_i(t, r)$ is independent of r. We rather make the assumption that G_i has separate variables, that is,

$$G_i(t, r) = g_i f(t) h(r) \quad (10)$$

for all $t \in [0, T]$ and all $r \in [r_i^{\min}, r_i^{\max}]$, where g_i is a constant (either positive or negative, depending on whether crystals of shape η_i are appearing or disappearing), and f and h do not depend on i.

Remark 2.1: In modelling the growth rate G_i, it can be linked with individual crystal volume growth. For r the radius of an individual crystal, the volume of an individual crystal is $V = \frac{4}{3}\pi\eta r^3$. As a consequence, $\frac{dV}{dt} = 4\pi\eta r^2 G_i$. This leads to choices such as $h(r) = 1/r^2$ for linear volume growth, or $h(r) = 1$ for volume growth proportional to the crystal surface (which corresponds to McCabe hypothesis).

Denote by $L^2(r_i^{\inf}, r_i^{\sup})$ the set of square integrable real-valued functions over $(r_i^{\inf}, r_i^{\sup})$, and $H^p(r_i^{\inf}, r_i^{\sup})$ the usual real-valued Sobolev spaces for $p \in \mathbb{N}$.

Theorem 2.2 (Well-posedness): Assume that $f \in C^0([0, T]; \mathbb{R})$ has a finite number of zeros and h is Lipschitz over $[r_i^{\min}, r_i^{\max}]$ and has constant sign. Then for all $\psi_{i,0} \in L^2(r_i^{\inf}, r_i^{\sup})$, there exists a unique solution $\psi_i \in C^0([0, T]; L^2(r_i^{\inf}, r_i^{\sup}))$ of the Cauchy problem (9).

Proof: Let n be the number of zeros of f and $([t_k, t_{k+1}])_{1\leq k\leq n}$ be intervals on which f has constant sign, with $t_1 = 0$ and $t_n = T$. Over each interval $[t_k, t_{k+1}]$, introduce the time reparametrization $\tilde{t} = \int_{t_k}^t |f(s)|\mathrm{d}s$. Then ψ is a solution of (9) over $[t_k, t_{k+1}]$ if and only if $\tilde{\psi}(\tilde{t}) = \psi(t)$ is a solution

$$\frac{\partial \tilde{\psi}_i}{\partial \tilde{t}}(\tilde{t}, r) + (\operatorname{sign} f) g_i h(r) \frac{\partial \tilde{\psi}_i}{\partial r}(\tilde{t}, r) = 0 \quad (11)$$

According to [5, Appendix 1], this linear hyperbolic system with periodic boundary conditions admits a unique solution in $C^0([t_k, \int_{t_k}^{t_{k+1}} |f(s)|\mathrm{d}s]; L^2(r_i^{\inf}, r_i^{\sup}))$. Reasoning by induction on each interval $[t_k, t_{k+1}]$, we find that there exists a unique $\psi_i \in C^0([0, T]; L^2(r_i^{\inf}, r_i^{\sup}))$ solution of (9). ■

Remark 2.3: If $\psi_{i,0}$ and f are more regular, then the corresponding solutions of (9) are also more regular. In particular, if $\psi_{i,0} \in H^2(r_i^{\inf}, r_i^{\sup})$ and $f \in C^2([0, T], \mathbb{R})$, then $\psi_i \in C^0([0, T]; H^2(r_i^{\inf}, r_i^{\sup})) \cap C^1([0, T]; H^1(r_i^{\inf}, r_i^{\sup})) \cap C^2([0, T]; L^2(r_i^{\inf}, r_i^{\sup}))$. This remark will be used in Theorem 3.2.

Now, let us recall the model of the accessible measurement, the CLD, denoted by q, given in [8]. For any $t \in [0, T]$, $\int_{\ell_1}^{\ell_2} q(t, \ell)\mathrm{d}\ell$ is the number of chords measured by the sensor at time t with length ℓ between ℓ_1 and ℓ_2. The cumulative CLD is given by $Q(t, \ell) = \int_0^\ell q(t, l)\mathrm{d}l$. We model the PSD-to-CLD relation by

$$Q(t, \ell) = \int_{r_1^{\min}}^{r_1^{\max}} k_1(\ell, r)\psi_1(t, r)\mathrm{d}r + \int_{r_2^{\min}}^{r_2^{\max}} k_2(\ell, r)\psi_2(t, r)\mathrm{d}r \quad (12)$$

where k_i is the kernel for the PSD-to-CLD of each crystal shape i. As developed [8], the apparent shape of a crystal with respect to the sensor is that of an ellipse (by projection onto a plane). In that way, for a given ellipse in the plane, the probability that the measured chord-length is less than ℓ is $1 - \sqrt{1 - \alpha\ell^2/(4r^2)}$, with coefficient $\alpha > 0$ depending on orientation and eccentricity of the ellipse (with maximum possible chord length $2r/\sqrt{\alpha}$). The apparent ellipse is linked to the shape of the crystal and the crystal's random orientation in the suspension, which follows a uniform distribution on the sphere given in spherical coordinates by the probability measure $\frac{\sin\theta}{4\pi}\mathrm{d}\phi\mathrm{d}\theta$ for $(\phi, \theta) \in [0, 2\pi] \times [0, \pi]$. The kernel k_i is obtained by total expectation over possible orientations:

$$k_i(\ell, r) = 1 - \int_{\phi=0}^{2\pi} \int_{\theta=0}^{\pi} \sqrt{1 - \frac{\ell^2}{4r^2}\alpha_{\eta_i}(\phi, \theta)} \frac{\sin\theta}{4\pi}\mathrm{d}\theta\mathrm{d}\phi, \quad (13)$$

with

$$\alpha_{\eta_i}(\phi, \theta) = \frac{\cos^2\phi}{\cos^2\theta + \eta_i^2\sin^2\theta} + \sin^2\phi \quad (14)$$

and the convention that $\sqrt{x}=0$ for $x<0$. Expression (12) comes from the law of total expectation, while kernels k_i can be determined by a probabilistic analysis of the two sources of hazards in the measure of a chord on a spheroid crystal: the random orientation of the spheroid with respect to the probe, and the random chord measured by the sensor on the projection of the spheroid onto the plane that is orthogonal to the probe's laser beam. Note that in the particular case of spherical crystals (*i.e.* $\eta=1$), expression (13) is simpler since $\alpha_1(\phi,\theta)=1$.

For a given shape η, the length of the largest chord possibly measured by the sensor on a crystal of size r is $\ell^{\max}=2r\max\{1,\eta\}$, since the direction of the largest diameter of a spheroid depends on whether $\eta>1$ or not. Set $\ell^{\max}=2\max\{r_1^{\max}\max\{1,\eta_1\},r_2^{\max}\max\{1,\eta_2\}\}$. Let $X_i=L^2(r_i^{\inf},r_i^{\sup})$ be the function spaces of PSDs and $Y=L^2(0,\ell^{\max})$ the function space of CLD. Define the operator $\mathcal{K}:X_1\times X_2\to Y$ that maps PSDs to their corresponding CLD:

$$\mathcal{K}(\psi_1,\psi_2)=\left(Q:\ell\mapsto\sum_{i=1}^{2}\int_{r_i^{\min}}^{r_i^{\max}}k_i(\ell,r)\psi_i(r)\mathrm{d}r\right). \tag{15}$$

The estimation problem that we aim to solve in this paper is the following: "From the knowledge of $Q(t)=\mathcal{K}(\psi_1(t),\psi_2(t))$ over $[0,T]$, where (ψ_1,ψ_2) is a solution of (9), estimate $(\psi_{1,0},\psi_{2,0})$."

III. Observability analysis

First, we need to determine if the CLD Q contains enough information to reconstruct the two PSDs ψ_1 and ψ_2. In other words, we investigate the observability of the PDE (9) with measured output Q. Several observability notions exist on infinite-dimensional systems.

Definition 3.1 (Observability): Let (ψ_1,ψ_2) be a solution of (9) and Q be the corresponding CLD. Let $W(T)=\int_0^T\|Q(t)\|_Y^2\mathrm{d}t$. System (9) is said to be

- exactly observable if, for some $\kappa>0$, $W(T)\geq\kappa(\|\psi_{1,0}\|_{X_1}^2+\|\psi_{2,0}\|_{X_2}^2)$ for all $\psi_{i,0}\in X_i$;
- approximately observable if $W(T)>0$ for all $(\psi_{1,0},\psi_{2,0})\neq(0,0)$.

These two notions are widely discussed in [24] for example. Clearly, exact observability implies approximate observability, and they are equivalent on finite dimensional systems. Unfortunately, the function $k_i(\ell,r)$ being bounded, the system is not exactly observable according to [6, Proposition 6.3]. Therefore, we focus on approximate observability, as in [10], [13], [28], and more recently in [6]. Let

$$A(\eta)=\begin{cases}1 & \text{if } \eta\geq 1,\\ 1/\eta^2 & \text{if } \eta<1.\end{cases}$$

We prove approximate observability under the following geometric condition

$$(r_1^{\min})^2A(\eta_2)\neq(r_2^{\min})^2A(\eta_1). \tag{16}$$

Theorem 3.2: Assume (16) holds. Assume $f\in C^2([0,T];\mathbb{R})$ has a finite number of zeros and $h(r)=1/r^m$ for some $m\in\mathbb{N}$. Let $\psi_{i,0}\in H^2(r_i^{\inf},r_i^{\sup})$ and denote by ψ_i for $i=1,2$ the corresponding solution of (9), satisfying the condition (3). If $\mathcal{K}(\psi_1(t,\cdot),\psi_2(t,\cdot))=0$ for all $t\in[0,T]$, then $(\psi_1,\psi_2)=(0,0)$.

Remark 3.3: This statement generalizes the result of [8], which was limited to the case where $1=\eta_1<\eta_2$, $r_1^{\min}(0)=r_2^{\min}(0)$, $r_1^{\max}(0)=r_2^{\max}(0)$, $g_1>0$, $g_2>0$ and $h(r)=1$. This case, not included in the statement of Theorem 3.2, can be recovered thanks to technical comments found in Remark 3.4.

We prove Theorem 3.2 in two steps. First the observability condition is translated into a sequential equality. Then we prove that this equality between sequences is actually asymptotically incompatible.

Step 1: From observability to sequence comparisons.

From (13), we can derive (from the power series expansion of $\ell\mapsto\sqrt{1-\ell^2}$) a power series expansion at 0 (with infinite convergence radius) of $\mathcal{K}_i$,

$$\mathcal{K}_i(\psi_i)(\ell)=\sum_{n=1}^{\infty}a_n(\eta_i)b_n\mathcal{F}_i^{2n}(\psi_i)\ell^{2n}$$

with $a_n(\eta)=\int_{\phi=0}^{2\pi}\int_{\theta=0}^{\pi}\alpha_\eta^n(\phi,\theta)\frac{\sin\theta}{4\pi}\mathrm{d}\theta\mathrm{d}\phi$, $b_n=\frac{1}{(n!)^2(1-2n)4^{2n}}$ and

$$\mathcal{F}_i^n(\psi_i)=\int_{r_i^{\min}}^{r_i^{\max}}\frac{\psi_i(r)}{r^n}\mathrm{d}r.$$

In proving the approximate observability, we may as well assume

$$\mathcal{K}_1(\psi_1(t))=\mathcal{K}_2(\psi_2(t)),\qquad t\in[0,T]. \tag{17}$$

This is reduced to power series expansion comparisons. Term-wise, we have

$$a_n(\eta_1)\mathcal{F}_1^{2n}(\psi_1)=a_n(\eta_2)\mathcal{F}_2^{2n}(\psi_2). \tag{18}$$

If $f(t)\neq 0$ (f is continuous and vanishes finitely many times), we differentiate (17) with respect to time to obtain

$$\frac{1}{f(t)}\partial_t\left(\frac{1}{f(t)}\partial_t\left(\mathcal{K}_1(\psi_1)\right)\right)=\frac{1}{f(t)}\partial_t\left(\frac{1}{f(t)}\partial_t\left(\mathcal{K}_2(\psi_2)\right)\right).$$

Since $\frac{1}{f(t)}\partial_t\left(\frac{1}{f(t)}\partial_t\psi_i\right)=g_i^2h(r)\partial_r(h(r)\partial_r\psi_i)$ (for $i=1,2$), we obtain

$$g_1^2a_n(\eta_1)\mathcal{F}_1^{2n}(h\partial_r(h\partial_r\psi_1))=g_2^2a_n(\eta_2)\mathcal{F}_2^{2n}(h\partial_r(h\partial_r\psi_2)), \tag{19}$$

where, again,

$$\mathcal{F}_i^{2n}(h\partial_r(h\partial_r\psi_i))=\int_{r_i^{\min}}^{r_i^{\max}}\frac{h(r)\partial_r(h(r)\partial_r\psi_i(r))}{r^{2n}}\mathrm{d}r.$$

Notation: To unburden the notations, we will denote $r_i=r_i^{\min}$ for the remaining of the section.

With $h(r) = 1/r^m$ and by integration by parts,

$$\begin{aligned}\mathcal{F}_i^{2n}(h\partial_r(h\partial_r\psi_i)) = &-\frac{\partial_r\psi_i(r_i)}{r_i^{2n+2m}} \\ &+ (2n+m)\mathcal{F}_i^{2n+2m+1}(\partial_r\psi_i) \\ = &-\frac{\partial_r\psi_i(r_i)}{r_i^{2n+2m}} - (2n+m)\frac{\psi_i(r_i)}{r_i^{2n+2m+1}} \\ &+ (2n+m)(2n+2m+1)\mathcal{F}_i^{2n+2m+2}(\psi_i)\end{aligned}$$

That is, changing the variable n to $n-m$,

$$\begin{aligned}\mathcal{F}_i^{2(n-m)}(h\partial_r(h\partial_r\psi_i)) = &-\frac{\partial_r\psi_i(r_i)}{r_i^{2n}} - (2n-m)\frac{\psi_i(r_i)}{r_i^{2n+1}} \\ &+ (2n-m)(2n+1)\mathcal{F}_i^{2n+2}(\psi_i). \quad (20)\end{aligned}$$

Now we express (19) in terms of (20):

$$\begin{aligned}&\frac{g_2^2}{g_1^2}\frac{a_{n-m}(\eta_2)}{a_{n-m}(\eta_1)}\Big[-\frac{\partial_r\psi_2(r_2)}{r_2^{2n}} - (2n-m)\frac{\psi_2(r_2)}{r_2^{2n+1}} \\ &\qquad + (2n-m)(2n+1)\mathcal{F}_1^{2n+2}(\psi_2)\Big] \\ &\quad = -\frac{\partial_r\psi_1(r_1)}{r_1^{2n}} - (2n-m)\frac{\psi_1(r_1)}{r_1^{2n+1}} \\ &\qquad + (2n-m)(2n+1)\mathcal{F}_1^{2n+2}(\psi_1).\end{aligned}$$

Finally, we switch $\mathcal{F}_2^{2n+2}(\psi_2)$ for $\mathcal{F}_1^{2n+2}(\psi_1)$ using (18), leading to the sequence equality

$$U_n = V_n, \qquad \forall n \geq m+1, n \in \mathbb{N}, \tag{21}$$

where we have set

$$U_n = \frac{g_2^2}{g_1^2}\frac{a_{n-m}(\eta_2)}{a_{n-m}(\eta_1)}\Big(-\frac{\partial_r\psi_2(r_2)}{r_2^{2n}} - (2n-m)\frac{\psi_2(r_2)}{r_2^{2n+1}}\Big)$$

$$\begin{aligned}V_n = &-\frac{\partial_r\psi_1(r_1)}{r_1^{2n}} - (2n-m)\Bigg[\frac{\psi_1(r_1)}{r_1^{2n+1}} + (2n+1)\times \\ &\Big(1 - \frac{g_2^2}{g_1^2}\frac{a_{n-m}(\eta_2)}{a_{n+1}(\eta_2)}\frac{a_{n+1}(\eta_1)}{a_{n-m}(\eta_1)}\Big)\mathcal{F}_1^{2n+2}(\psi_1)\Bigg].\end{aligned}$$

Step 2: Asymptotical identities.

To prove the approximate observability result, we prove that the asymptotics of both sides of (21) are incompatible, imposing $(\psi_1, \psi_2) = (0, 0)$. To achieve the comparison, we need three identities. First, if $\psi_i(r_i) \neq 0$, then

$$\mathcal{F}_i^{2n}(\psi_i) \sim \frac{\psi_i(r_i)}{2nr_i^{2n-1}}. \tag{22}$$

This can be obtained by comparing $\psi_i(r)$ to $\psi_i(r_i)$ on any small interval $(r_i, r_i+\delta)$ $(\delta > 0)$. By integration by parts, we also get that if $\psi_i(r_i) = 0$ but $\partial_r\psi_i(r_i) \neq 0$, then

$$\mathcal{F}_i^{2n}(\psi_i) \sim \frac{\partial_r\psi_i(r_i)}{4n^2r_i^{2n-2}}. \tag{23}$$

Finally, we have $\lim_{n\to+\infty}\frac{a_{n+1}(\eta)}{a_n(\eta)} = A(\eta)$. This can be obtained thanks to the following remark. The function $(\phi,\theta) \mapsto \frac{\sin\theta}{4\pi}$ is the density of a probability measure μ on $(\phi,\theta) \in [0, 2\pi] \times [0, \pi]$. As such, $a_n(\eta) = \mathbb{E}\left(\alpha_\eta^n\right)$ where $\mathbb{E}$ denotes the expected value with respect to μ. In that respect,

$$a_{n+1}(\eta) = \mathbb{E}\left(\alpha_\eta^{n+1}\right) \leq \|\alpha_\eta\|_\infty \mathbb{E}\left(\alpha_\eta^n\right) = \|\alpha\|_\infty a_n(\eta).$$

On the other hand, Jensen's inequality for μ yields

$$a_{n+1}(\eta) = \mathbb{E}\left(\left(\alpha_\eta^n\right)^{\frac{n+1}{n}}\right) \geq \left(\mathbb{E}\left(\alpha_\eta^n\right)\right)^{1+\frac{1}{n}} = (a_n(\eta))^{1+\frac{1}{n}}.$$

Hence $(a_n(\eta))^{\frac{1}{n}} \leq \frac{a_{n+1}(\eta)}{a_n(\eta)} \leq \|\alpha_\eta\|_\infty$. We obtain the result by noticing that both sides converge to $\|\alpha_\eta\|_\infty = A(\eta)$.

Step 3: Proof of Theorem 3.2.

Proof: First, let us analyse the influence of border terms.

Assuming either $\psi_2(r_2) \neq 0$ or $\partial_r\psi_2(r_2) \neq 0$, the quotient U_{n+1}/U_n, yields

$$\begin{aligned}&\frac{\partial_r\psi_2(r_2)r_2 + (2n+2-m)\psi_2(r_2)}{\partial_r\psi_2(r_2)r_2^3 + (2n-m)\psi_2(r_2)r_2^2}\times \\ &\qquad\qquad \frac{a_{n-m+1}(\eta_2)}{a_{n-m}(\eta_2)}\frac{a_{n-m}(\eta_1)}{a_{n-m+1}(\eta_1)},\end{aligned}$$

which has limit $\frac{A(\eta_2)}{r_2^2A(\eta_1)}$.

For the treatment of V_n, we use a natural generalization of the limit quotient of a_n:

$$\frac{a_{n-m}(\eta_2)}{a_{n+1}(\eta_2)}\frac{a_{n+1}(\eta_1)}{a_{n-m}(\eta_1)} \to \frac{A(\eta_1)^{m+1}}{A(\eta_2)^{m+1}}.$$

If $\psi_1(r_1) \neq 0$, then we deduce from (22) that $\frac{V_nr_1^{2n}}{2n}$ has limit $-\frac{g_2^2}{g_1^2}\frac{A(\eta_1)^{m+1}}{A(\eta_2)^{m+1}}\psi_1(r_1)$, which is incoherent with a limit quotient of $\frac{A(\eta_2)}{r_2^2A(\eta_1)} \neq \frac{1}{r_1^2}$ by assumption (16).

If $\psi_i(r_i) = 0$ but $\partial_r\psi_i(r_i) \neq 0$, then we deduce from (22) that $\frac{V_nr_1^{2n}}{4n^2}$ has limit $-\frac{g_2^2}{g_1^2}\frac{A(\eta_1)^{m+1}}{A(\eta_2)^{m+1}}\partial_r\psi_1(r_1)$ which is again incoherent with a limit quotient of $\frac{A(\eta_2)}{r_2^2A(\eta_1)} \neq \frac{1}{r_1^2}$.

Hence having $\psi_2(r_2) \neq 0$ or $\partial_r\psi_2(r_2) \neq 0$, is incoherent with having $\psi_1(r_1) \neq 0$ or $\partial_r\psi_1(r_1) \neq 0$. Now let's assume that $\psi_2(r_2) = \partial_r\psi_2(r_2) = 0$. Then if $\psi_1(r_1) \neq 0$, the $\frac{V_nr_1^{2n}}{2n}$ has a non-zero limit despite being constantly zero, which is excluded. The same goes if $\partial\psi_1(r_1) \neq 0$ while $\psi_1(r_1) = 0$.

The conclusion of this first step is that if there exists a pair (ψ_1, ψ_2) of C^2 functions satisfying (21), they must satisfy

$$\psi_1(r_1) = \partial_r\psi_1(r_1) = \psi_2(r_2) = \partial_r\psi_2(r_2) = 0.$$

We are now in a suitable position to conclude focusing on interior terms. In that case, we are left with the equality

$$\left(1 - \frac{g_2^2}{g_1^2}\frac{a_{n-m}(\eta_2)}{a_{n+1}(\eta_2)}\frac{a_{n+1}(\eta_1)}{a_{n-m}(\eta_1)}\right)\mathcal{F}_1^{2n+2}(\psi_1) = 0.$$

Naturally, $\mathcal{F}_1^{2n+2}(\psi_1)$ must have infinitely many non-zero terms, otherwise $\psi_1 = 0$ (the family $(1/r^{2n})_{n\geq n_0}$ is total on any bounded interval in (a, b), $0 < a < b$, for any n_0). But this would imply that

$$\frac{a_{n-m}(\eta_2)}{a_{n+1}(\eta_2)}\frac{a_{n+1}(\eta_1)}{a_{n-m}(\eta_1)} = \frac{g_1^2}{g_2^2}.$$

infinitely often, which is not true except if $\eta_1 = \eta_2$ and $g_1 = g_2$. ■

Remark 3.4: In the case $r_1 = r_2$, $\eta_1 = 1$ and $\eta_2 > 1$, Theorem 2.2 does not allow to answer but the approximate observability result still holds due the following observation. In that case, $a_n(\eta_2) \to 0$ but $1 > a_n(\eta_2) \geq 1/\sqrt{n}$. Hence, in (21), $V_n \times r_1^{2n}$ is equivalent to an integer power in n, while $U_n \times r_1^{2n}$ cannot, because of the dominating term containing $a_{n-m}(\eta_2)$.

IV. Observer and numerical simulations

The observability analysis of the previous section guarantees the convergence of the state estimation by a BFN algorithm. Recall that the goal is to estimate $\psi_{i,0}$ from the measurement of the CLD Q over $[0, T]$. The BFN algorithm consists in applying iteratively of forward and backward Luenberger observers. After each iteration of an observer over $[0, T]$, the final estimation obtained at T is used as the initial condition of the next observer. This strategy has been used in various contexts in recent decades [2]–[4]. As shown in [13] (which extended the results of [14], [23] which focused on exactly observable systems), the type of convergence depends on the observability properties of the system. These results have been extended to the non-autonomous context (which is the case here since G_i is time-varying) in [6] and applied to a crystallization process in [8].

In the context of this paper, the forward and backward observers are given by:

$$\begin{cases} \dfrac{\partial \hat{\psi}_i^{2n}}{\partial t}(t,r) = -G_i(t,r)\dfrac{\partial \hat{\psi}_i^{2n}}{\partial r}(t,r) \\ \qquad\qquad - \mu\mathcal{K}^*(\mathcal{K}(\hat{\psi}_1^{2n}(t), \hat{\psi}_2^{2n}(t)) - Q(t)) \\ \hat{\psi}_i^{2n}(0,r) = \begin{cases} \hat{\psi}_i^{2n-1}(0,r) & \text{if } n \geq 1 \\ \hat{\psi}_{i,0}(r) & \text{otherwise} \end{cases} \end{cases} \tag{24}$$

$$\begin{cases} \dfrac{\partial \hat{\psi}_i^{2n+1}}{\partial t}(t,r) = -G_i(t,r)\dfrac{\partial \hat{\psi}_i^{2n+1}}{\partial r}(t,r) \\ \qquad\qquad + \mu\mathcal{K}^*(\mathcal{K}(\hat{\psi}_1^{2n+1}(t), \hat{\psi}_2^{2n+1}(t)) - Q(t)) \\ \hat{\psi}_i^{2n+1}(T,r) = \hat{\psi}_i^{2n}(T,r) \end{cases} \tag{25}$$

where $\hat{\psi}_i^n(t,r)$ represents the estimation of $\psi_i(t,r)$ obtained by the algorithm after n iterations, $Q(t) = \mathcal{K}(\psi_1(t), \psi_2(t))$ is the CLD at time t, μ is a degree of freedom, called the observer gain, and $\mathcal{K}^*$ is the adjoint of the operator $\mathcal{K}$:

$$\begin{array}{rccl} \mathcal{K}^*: & Y & \longrightarrow & X_1 \times X_2 \\ & Q & \longmapsto & \left(r \mapsto \int_0^{\ell^{\max}} k_i(\ell, r) Q(\ell) \mathrm{d}\ell\right)_{1 \leq i \leq 2}. \end{array}$$

Note that (24) is the usual infinite-dimensional Luenberger observer of (9), while (25) is a Luenberger observer of (9) when reversed in time. Then, combining the observability analysis provided in Theorem 3.2 and the convergence result [8, Theorem 4.2], we obtain the following result.

Theorem 4.1: Under the assumptions of Theorem 3.2, for all $\mu > 0$, all $t \in [0, T]$ and almost all $r \in [r_0, r_1]$,

$$\hat{\psi}^n(t,r) \underset{n \to +\infty}{\longrightarrow} \psi(t,r). \tag{26}$$

We propose a numerical simulation of this algorithm. System (9) and observer (24)-(25) being transport equations, they are solved by the method of characteristics. The characteristic equation is given by

$$\frac{\mathrm{d}\rho_i}{\mathrm{d}t} = G_i(t, \rho_i(t)). \tag{27}$$

Along the solutions of this ODE, ψ_i and $\hat{\psi}_i^n$ satisfy

$$\frac{\mathrm{d}}{\mathrm{d}t}\psi_i(t, \rho_i(t)) = 0, \tag{28}$$

$$\frac{\mathrm{d}}{\mathrm{d}t}\hat{\psi}_i^n(t, \rho_i(t)) = (-1)^{2n+1}\mu\mathcal{K}^*(\mathcal{K}(\hat{\psi}_1^n(t), \hat{\psi}_2^n(t)) - Q(t)). \tag{29}$$

We choose a spatial discretization of $[r_i^{\inf}, r_i^{\sup}]$ with space-step $\mathrm{d}x$, and integrate the characteristic equation (27) over $[0, T]$ with time-step $\mathrm{d}t$ with initial conditions in this spatial discretization. Then, we integrate ODEs (28)-(29) along the characteristic curves with a first order Euler method. Concerning the operator $\mathcal{K}$, integrals are computed with the rectangles methods. We consider the set of parameters given in Table I, and the observer gain $\mu = 0.001$ (small enough to preserve stability of the numerical scheme). Note that in this example, G does not depends on t, but this actually does not affect the convergence properties, since it is always possible to use a time-reparametrization as it is done in the proof of Theorem 2.2. Moreover, condition (16) is satisfied by the example.

$r_1^{\min} = r_2^{\min} = 0.1$	$r_1^{\max} = r_2^{\max} = 0.2$	$T = 1$
$g_1 = 0.1$	$g_2 = 0.2$	$f(t)h(r) = 1/r^2$
$\eta_1 = 0.5$	$\eta_2 = 2$	$\mathrm{d}x = \mathrm{d}t = 0.01$

TABLE I

Parameters of the numerical simulation.

The observer is initialized at $\hat{\psi}_{1,0} = \hat{\psi}_{2,0} = 0$. The initial conditions $\psi_{1,0}$ and $\psi_{2,0}$ are chosen as normal distributions centered at $r = 0.05$ and $r = 0.15$, respectively. Roughly speaking, crystals of shape η_1 will appear during $[0, T]$, but are not in the reactor at $t = 0$, while crystals of shape η_2 are in the reactor at $t = 0$ but disappear through the process. The result of the simulation is presented in Figure 1 (numerical implementation can be found in repository [9]). After only 10 iterations, the locus of the maximum of the two PSDs is already well estimated. In practice, this is the main information to be estimated. After 1000 iterations, the estimations are much more accurate. Still, a peak at $r = 0.15$ remains on $\hat{\psi}_{1,0}$ while it is not in $\psi_{1,0}$. This peak is due to the important contribution of $\psi_{2,0}$ in the CLD at $r = 0.15$. However, its amplitude decreases as the number of iterations increases, and eventually vanishes according to Theorem 4.1.

V. Conclusion

In this paper, we propose an observability analysis of a crystallization process. We prove, under a geometric condition, that two PSDs of spheroid crystals of different shapes are fully determined by their common CLD along the process. Hence, the BFN algorithm is able to reconstruct the

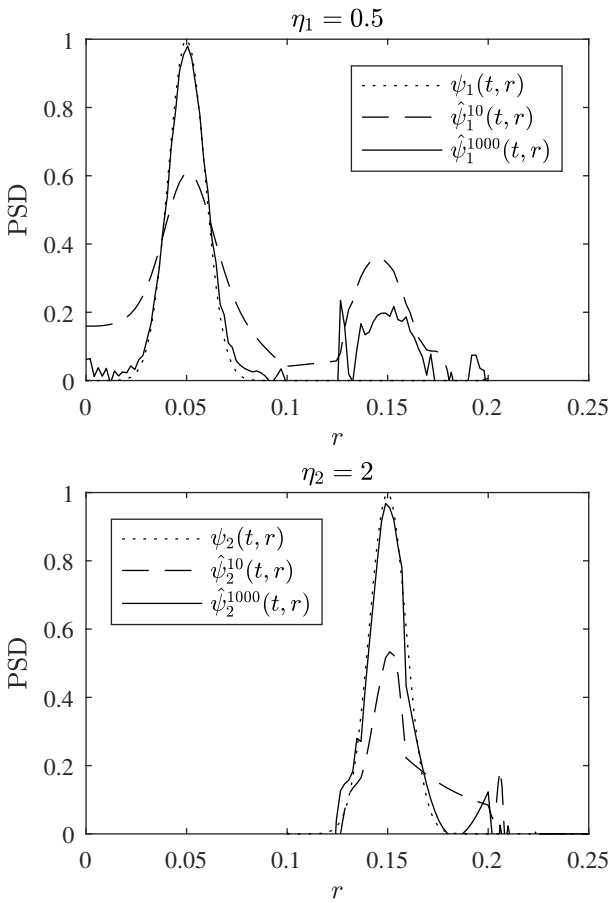

Fig. 1. PSDs ψ_1 and ψ_2 at time $t = 0$ and their estimations $\hat{\psi}_1^{2n}(0)$ and $\hat{\psi}_2^{2n}(0)$ obtained after 20 and 100 iterations of the BFN algorithm.

PSDs from the measurement of the CLD over a finite time interval, by using iterations of forward and backward infinite-dimensional Luenberger observers. We provide a numerical simulation of the algorithm which suggest that possible applications of this method to experimental data could benefit from this theoretical study.

REFERENCES

[1] Okpeafoh S. Agimelen, Peter Hamilton, Ian Haley, Alison Nordon, Massimiliano Vasile, Jan Sefcik, and Anthony J. Mulholland. Estimation of particle size distribution and aspect ratio of non-spherical particles from chord length distribution. *Chemical Engineering Science*, 123:629 – 640, 2015.

[2] Didier Auroux and Jacques Blum. Back and forth nudging algorithm for data assimilation problems. *C. R. Math. Acad. Sci. Paris*, 340(12):873–878, 2005.

[3] Didier Auroux and Jacques Blum. A nudging-based data assimilation method: the back and forth nudging (bfn) algorithm. *Nonlinear Processes in Geophysics*, 15(2):305–319, 2008.

[4] Didier Auroux and Maëlle Nodet. The back and forth nudging algorithm for data assimilation problems: theoretical results on transport equations. *ESAIM Control Optim. Calc. Var.*, 18(2):318–342, 2012.

[5] Georges Bastin and Jean-Michel Coron. *Stability and boundary stabilization of 1-d hyperbolic systems*, volume 88. Springer, 2016.

[6] Lucas Brivadis, Vincent Andrieu, Ulysse Serres, and Jean-Paul Gauthier. Luenberger observers for infinite-dimensional systems, back and forth nudging, and application to a crystallization process. *SIAM Journal on Control and Optimization*, 59(2):857–886, 2021.

[7] Lucas Brivadis, Vincent Andrieu, Élodie Chabanon, Émilie Gagnière, Noureddine Lebaz, and Ulysse Serres. New dynamical observer for a batch crystallization process based on solute concentration. *Journal of Process Control*, 87:17 – 26, 2020.

[8] Lucas Brivadis and Ludovic Sacchelli. New inversion methods for the single/ multi-shape CLD-to-PSD problem with spheroid particles. Submitted to *Journal of Process Control*. Under review., December 2020.

[9] Lucas Brivadis and Ludovic Sacchelli. Project BFNCrist. https://github.com/sacchelli/BFNCrist, 2021.

[10] F. Celle, J.-P. Gauthier, D. Kazakos, and G. Sallet. Synthesis of nonlinear observers: a harmonic-analysis approach. *Math. Systems Theory*, 22(4):291–322, 1989.

[11] Zhenguo Gao, Yuanyi Wu, Ying Bao, Junbo Gong, Jingkang Wang, and Sohrab Rohani. Image analysis for in-line measurement of multidimensional size, shape, and polymorphic transformation of l-glutamic acid using deep learning-based image segmentation and classification. *Crystal Growth & Design*, 18(8):4275–4281, 08 2018.

[12] Frédéric Gruy. Chord Length Distribution: relationship between Distribution Moments and Minkowski Functionals. Preprint, 2017.

[13] Ghislain Haine. Recovering the observable part of the initial data of an infinite-dimensional linear system with skew-adjoint generator. *Math. Control Signals Systems*, 26(3):435–462, 2014.

[14] Kazufumi Ito, Karim Ramdani, and Marius Tucsnak. A time reversal based algorithm for solving initial data inverse problems. *Discrete Contin. Dyn. Syst. Ser. S*, 4(3):641–652, 2011.

[15] Noureddine Lebaz, Arnaud Cockx, Mathieu Spérandio, and Jérôme Morchain. Reconstruction of a distribution from a finite number of its moments: A comparative study in the case of depolymerization process. *Computers & Chemical Engineering*, 84, 09 2015.

[16] Weidong Liu, Nigel N Clark, and Ali Ihsan Karamavruç. Relationship between bubble size distributions and chord-length distribution in heterogeneously bubbling systems. *Chemical Engineering Science*, 53(6):1267–1276, 1998.

[17] A. Mersmann, A. Eble, and C. Heyer. Crystal growth. In A. Mersmann, editor, *Crystallization Technology Handbook*, pages 48–111. Marcel Dekker Inc., 2001.

[18] Ali Mesbah, Adrie E.M. Huesman, Herman J.M. Kramer, and Paul M.J. Van den Hof. A comparison of nonlinear observers for output feedback model-based control of seeded batch crystallization processes. *Journal of Process Control*, 21(4):652–666, 2011.

[19] J.W. Mullin. *Crystallization*. Elsevier, 4 edition, 2001.

[20] Ajinkya V Pandit and Vivek V Ranade. Chord length distribution to particle size distribution. *AIChE Journal*, 62(12):4215–4228, 2016.

[21] Marcella Porru and Leyla Özkan. Monitoring of batch industrial crystallization with growth, nucleation, and agglomeration. part 2: Structure design for state estimation with secondary measurements. *Industrial & engineering chemistry research*, 56(34):9578–9592, 2017.

[22] Benoit Presles, Johan Debayle, Gilles Fevotte, and Jean-Charles Pinoli. Novel image analysis method for in situ monitoring the particle size distribution of batch crystallization processes. *Journal of Electronic Imaging*, 19(3):1 – 7, 2010.

[23] Karim Ramdani, Marius Tucsnak, and George Weiss. Recovering and initial state of an infinite-dimensional system using observers. *Automatica J. IFAC*, 46(10):1616–1625, 2010.

[24] Marius Tucsnak and George Weiss. *Observation and control for operator semigroups*. Birkhäuser Advanced Texts: Basel Textbooks. Birkhäuser Verlag, Basel, 2009.

[25] Basile Uccheddu, KUN Zhang, Hassan Hammouri, and Gilles Févotte. Design of a csd observer during batch cooling crystallization dealing with uncertain nucleation parameters. *IFAC Proceedings Volumes*, 44(1):10460–10465, 2011.

[26] Jochem Adrianus Wilhelmus Vissers. *Model-based estimation and control methods for batch cooling crystallizers*. PhD thesis, Technische Universiteit Eindhoven, 2012.

[27] Jörg Worlitschek, Thomas Hocker, and Marco Mazzotti. Restoration of psd from chord length distribution data using the method of projections onto convex sets. *Particle & Particle Systems Characterization*, 22(2):81–98, 2005.

[28] C.-Z. Xu, P. Ligarius, and J.-P. Gauthier. An observer for infinite-dimensional dissipative bilinear systems. *Comput. Math. Appl.*, 29(7):13–21, 1995.